Materials Advances

ROYAL SOCIETY OF CHEMISTRY

PAPER

View Article Online
View Journal | View Issue

Check for updates

Cite this: *Mater. Adv.*, 2025, **6**, 196

Origin and enhancement of the piezoelectricity in monolayer group IV monochalcogenides under strain and in the presence of vacancies

Arun Jangir,[a] Duc Tam Ho [b] and Udo Schwingenschlögl *[a]

Received 20th August 2024,
Accepted 11th November 2024

DOI: 10.1039/d4ma00837e

rsc.li/materials-advances

Piezoelectric materials are a critical component in many electronic devices from the nanoscale to the macroscale. Monolayer group IV monochalcogenides can provide particularly large piezoelectric coefficients. To investigate the origin of this strong piezoelectricity, we conduct an atomic-level analysis of the charge redistribution under mechanical strain. Our results show that it arises from charge transfer between strong and weak chemical bonds. We demonstrate that the piezoelectric coefficients can be substantially enhanced by mechanical strain and the presence of vacancies, for instance in the case of monolayer SnSe by up to 112% by 2% compression and by up to 433% by an Sn–Se vacancy density of 5.5%.

1. Introduction

Electro-mechanical coupling (piezoelectricity), which exists only in non-centrosymmetric materials, is the generation of deformation by an electric field, and *vice versa*. Piezoelectric materials have a wide range of applications from the nanoscale to the macroscale, such as accelerometers,[1] sensors,[2] resonators,[3] bioprobes,[4] nanogenerators,[5,6] actuators,[7] scaffolds,[8] and bone-growth stimulators.[9] While three-dimensional piezoelectric materials (organic, inorganic, composite, bio-inspired, *etc.*) and their nanostructures (nanotubes, nanowires, nanorings, *etc.*) are well known, the research on two-dimensional piezoelectric materials accelerates only since monolayer MoS_2 was shown to perform comparably to three-dimensional ZnO.[10–12] The possibility to tailor the properties of two-dimensional piezoelectric materials by methods such as stacking, functionalization, and defect engineering opens excellent prospects for their integration in future electro-mechanical systems.

Some monolayer materials exhibit intrinsic piezoelectricity, such as transition metal dichalcogenides,[13] group II oxides,[13] hexagonal III–V semiconductors,[13] group III monochalcogenides,[14] group IV monochalcogenides,[15–17] and α-In_2Se_3.[18] In addition, piezoelectric response can be induced extrinsically in graphene by ad-atom adsorption,[19] triangular cutting,[20] and bending.[21] The piezoelectric coefficients of the monolayer group IV monochalcogenides are several orders of magnitude higher than those of other two-dimensional materials due to their puckered structure,[15] which also allows the materials to sustain large strain without failure.[22] The atomistic mechanism leading to the high piezoelectric coefficients, however, is largely unknown. The same applies to the effect of vacancies, which hold great promise to enhance the piezoelectricity, as their concentration can be well controlled by lithiation.[23] For these reasons, we investigate in the present study the piezoelectric coefficients of the monolayer group IV monochalcogenides GeS, GeSe, SnS, and SnSe by first-principles calculations. Using geometrical, crystal orbital Hamilton population, and valence charge density analyses, we show that distinct charge transfer between strong and weak chemical bonds is the origin of the strong piezoelectricity and that this charge transfer can be enhanced by mechanical strain and the presence of vacancies.

2. Computational details

We perform first-principles calculations using the Vienna *ab initio* simulation package[24] (projector augmented wave method with 600 eV plane wave energy cutoff). The Perdew–Burke–Ernzerhof exchange correlation functional is adopted together with an energy convergence criterion of 10^{-7} eV, 16 × 16 × 1 Monkhorst–Pack *k*-grids for unit cells, and Monkhorst–Pack *k*-grids of the same density for supercells. All structures are relaxed using the variable cell method until no atomic force component exceeds 10^{-3} eV Å^{-1}. The polarization $P_i(\varepsilon_{jk})$, where ε_{jk} represents the strain and $i, j, k = 1$, 2, and 3 represents the x, y, and z-axis, respectively, is obtained by the Berry phase approach.[25,26] After second degree polynomial

[a] *Physical Science and Engineering Division, King Abdullah University of Science and Technology (KAUST), Thuwal 23955-6900, Saudi Arabia. E-mail: udo.schwingenschlogl@kaust.edu.sa*
[b] *Department of Mechanical and Construction Engineering, Northumbria University, Newcastle Upon Tyne NE1 8ST, UK*

fitting of $P_i(\varepsilon_{jk})$, the components of the piezoelectric tensor **e** are computed as[27]

$$e_{ijk} = \frac{\partial P_i(\varepsilon_{jk})}{\partial \varepsilon_{jk}} + \delta_{jk} P_i(0) - \delta_{ij} P_k(0), \quad (1)$$

where $P_i(\varepsilon_{jk})$ is taken as the spontaneous polarization, *i.e.*, with respect to a hypothetical non-polar structure in that the atoms are aligned at x = 0, 0.5, or 1. To obtain the components d_{ijk} of the piezoelectric tensor **d**, we utilize the elasticity tensor **C**,[15] which fulfills (Einstein notation)

$$e_{ijk} = d_{ilm} C_{lmjk}, \quad (2)$$

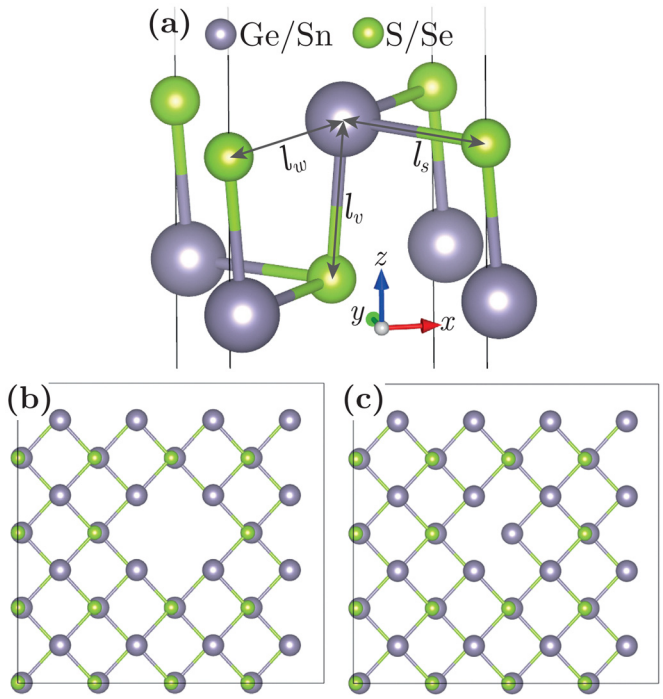

Fig. 1 (a) Crystal structure of the monolayer group IV monochalcogenides GeS, GeSe, SnS, and SnSe, where l_v, l_s, and l_w represent the bond lengths of the vertical, strong, and weak bonds, respectively. Top view of a 4 × 4 supercell of SnSe with (b) a pair of Sn and Se atoms removed (SnSe-p4) and (c) a single Se atom removed (SnSe-s4).

resulting in

$$d_{111} = \frac{e_{111} C_{2222} - e_{122} C_{1122}}{C_{1111} C_{2222} - C_{1122}^2} \quad (3)$$

and

$$d_{122} = \frac{e_{122} C_{1111} - e_{111} C_{1122}}{C_{1111} C_{2222} - C_{1122}^2}. \quad (4)$$

3. Results and discussion

Fig. 1(a) shows the atomic arrangement of the monolayer group IV monochalcogenides, which consist of two atomic layers forming a puckered structure. The armchair and zigzag directions are parallel to the *x*- and *y*-axes, respectively. The two atomic layers are connected by vertical bonds (l_v), whereas there are strong (l_s; short) and weak (l_w; long) intralayer bonds. Polarization is present along the *x*-axis, but not along the *y*-axis because of the mirror plane perpendicular to this axis. To study the effect of vacancies, a pair of Sn and Se atoms (Sn–Se vacancy) or a single Se atom is removed from 3 × 3, 4 × 4, and 5 × 5 supercells of SnSe (SnSe-p3, SnSe-p4, SnSe-p5, SnSe-s3, SnSe-s4, and SnSe-s5, respectively). The unrelaxed structures of SnSe-p4 and SnSe-s4 are shown in Fig. 1(b) and (c). Sn–Se and Se vacancies are observed experimentally[23] and first-principles calculations show that they maintain the semiconducting state.[28]

The relaxed lattice parameters, bond lengths, elastic constants, and piezoelectric coefficients of the investigated monolayers are summarized in Table 1. The results agree well with the e_{111} values of ref. 15 (5 × 10^{-10} C m^{-1} for GeS, 12 × 10^{-10} C m^{-1} for GeSe, 18 × 10^{-10} C m^{-1} for SnS, and 35 × 10^{-10} C m^{-1} for SnSe) but not with the e_{122} values of ref. 15 (−10 × 10^{-10} C m^{-1} for GeS, −8 × 10^{-10} C m^{-1} for GeSe, −14 × 10^{-10} C m^{-1} for SnS, and 11 × 10^{-10} C m^{-1} for SnSe), which is due to the fact that the second and third terms of eqn (1) are omitted in ref. 15. Both e_{111} and d_{111} are comparable to the literature values for F-AlN-H (e_{111} = 9 × 10^{-10} C m^{-1}, d_{111} = 16 pm V^{-1}),[29] $CrTe_2$ (e_{111} = 7 × 10^{-10} C m^{-1}, d_{111} = 13 pm V^{-1}),[14] TmS (e_{111} = 6 × 10^{-10} C m^{-1}, d_{111} = 61 pm V^{-1}),[30] Te_2Se (e_{111} = 5 × 10^{-10} C m^{-1}, d_{111} = 16 pm V^{-1}),[31] MoS_2 (e_{111} = 4 × 10^{-10} C m^{-1}, d_{111} = 4 pm V^{-1}),[32] CdO (e_{111} = 3 × 10^{-10} C m^{-1}, d_{111} = 22 pm V^{-1}),[14] ZnSiSSe (e_{111} = 3 × 10^{-10} C m^{-1}, d_{111} = 7 pm V^{-1}),[33] InN (e_{111} = 2 × 10^{-10} C m^{-1}, d_{111} = 6 pm V^{-1}),[14] BP (e_{111} = 2 × 10^{-10} C m^{-1}, d_{111} = 2 pm V^{-1}),[14] GaSe (e_{111} = 1 × 10^{-10} C m^{-1},

Table 1 Relaxed lattice parameters, bond lengths, elastic constants, and piezoelectric coefficients

	a (Å)	b (Å)	l_v (Å)	l_s (Å)	l_w (Å)	C_{1111} (N m^{-1})	C_{1122} (N m^{-1})	C_{2222} (N m^{-1})	e_{111} (10^{-10} C m^{-1})	e_{122} (10^{-10} C m^{-1})	d_{111} (pm V^{-1})	d_{122} (pm V^{-1})
GeS	4.47	3.66	2.43	2.48	3.37	13	19	45	7	−5	179	−86
GeSe	4.27	3.98	2.55	2.67	3.19	19	18	48	13	−3	121	−52
SnS	4.28	4.08	2.59	2.75	3.21	18	16	40	20	1	176	−70
SnSe	4.38	4.29	2.72	2.92	3.22	21	18	43	33	6	212	−73
SnSe-p3	12.96	12.93	—	—	—	21	13	27	53	32	257	−9
SnSe-p4	17.38	17.22	—	—	—	19	13	31	36	13	216	−47
SnSe-p5	21.74	21.52	—	—	—	21	15	36	40	13	237	−63
SnSe-s3	12.99	12.90	—	—	—	20	13	32	−34	−16	−190	30
SnSe-s4	17.33	17.23	—	—	—	21	14	34	−49	−19	−280	62
SnSe-s5	21.79	21.44	—	—	—	21	19	41	41	7	303	−125

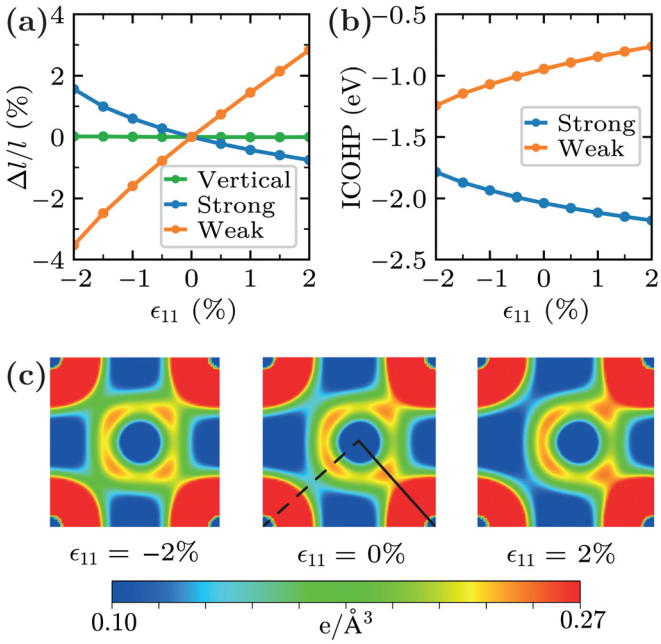

Fig. 2 (a) Variation of the bond lengths under strain. (b) Crystal orbital Hamilton population integrated up to the Fermi level for strong and weak bonds. (c) Valence charge density distribution at different strains in the top atomic layer of SnSe (Se atoms located at the corners). The solid and dashed lines indicate the strong and weak bonds, respectively.

d_{111} = 2 pm V^{-1}),[13] and PtSiSe ($e_{111} = -20 \times 10^{-10}$ C m^{-1}, d_{111} = −62 pm V^{-1}).[34]

We consider the effect of strain only in the case of SnSe, as the bonding is similar across the family and the findings thus can be generalized to the other members. Fig. 2(a) shows the variations of l_v, l_s, and l_w in response to −2% to 2% strain along the x-axis. The thickness of the monolayer changes by only 0.3% under the extremal applied strains. While generally applied strain may be released by changing both the bond lengths and bond angles, here the latter is energetically favorable, *i.e.*, l_v hardly changes. On the other hand, l_s decreases/increases under tensile/compressive strain and l_w shows the opposite behavior. The trend of l_s is counterintuitive, as it points to strengthening of the bond when the material is stretched along the x-axis. The strength of a bond can be evaluated by integrating the crystal orbital Hamilton population up to the Fermi level (ICOHP),[35] see the results in Fig. 2(b). The negative values represent bonding. Increasingly/decreasingly negative values of the strong bond under tensile/compressive strain imply increasing/decreasing bond strength. In contrast, the weak bond becomes weaker/stronger under tensile/compressive strain.

The valence charge density in the top atomic layer under compressive/tensile strain, see Fig. 2(c), decreases/increases along the strong bond (solid line) and increases/decreases along the weak bond (dashed line), establishing a significant charge transfer between the two bonds. The trends of l_s and l_w as well as the ICOHP comply with charge transfer from the weak/strong bond to the strong/weak bond under tensile/compressive strain. This charge transfer is the origin of the piezoelectricity. Table 1 shows that l_s increases significantly with the atomic sizes (Ge < Sn and S < Se), while l_w is much less affected due to the weakness of this intralayer bond. Thus, the difference between l_s and l_w follows the trend GeS > GeSe > SnS > SnSe, which explains the trend of the piezoelectric response across the family without strain as well as the decreasing/increasing slope of ΔP_1 under tensile/compressive strain in Fig. 3(a). As a consequence, compressive strain can be utilized to enhance the

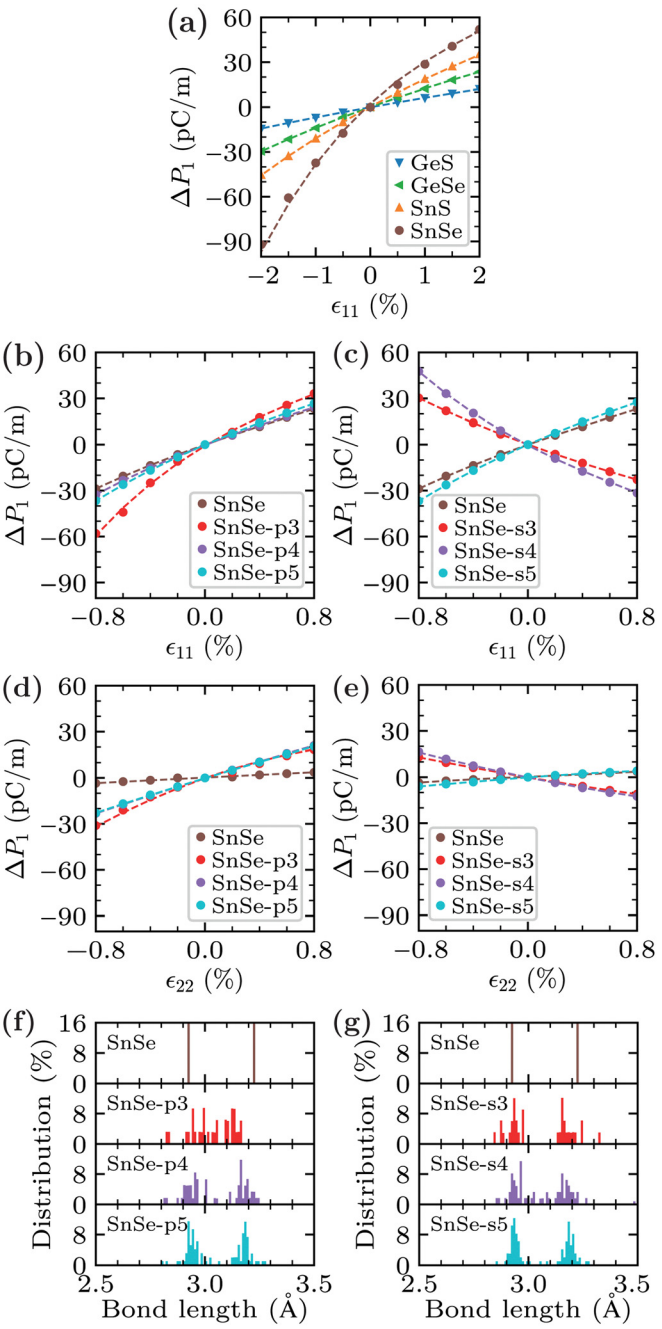

Fig. 3 Normalized polarization $\Delta P_1 = P_1(\varepsilon_{jk}) - P_1(0)$ under strain in (a) pristine monolayer GeS, GeSe, SnS, and SnSe as well as in monolayer SnSe with (b) and (d) Sn–Se and (c) and (e) Se vacancies. (f) and (g) Histograms of the intralayer bond lengths (l_s and l_w).

piezoelectric response, which, combined with the ability to withstand large strain, demonstrates excellent application potential of the materials under investigation. For instance, 2% compression of monolayer SnSe enhances e_{111} by 112%.

The presence of vacancies can significantly affect the charge density distribution and, thus, the charge transfer. We consider vacancy densities of 5.5% (SnSe-p3), 3.1% (SnSe-p4), 2.0% (SnSe-p5), 2.2% (SnSe-s3), 1.5% (SnSe-s4), and 1.0% (SnSe-s5). Table 1 shows that the piezoelectric coefficients of SnSe-p4 and SnSe-p5 are a bit higher than those of pristine monolayer SnSe, whereas those of SnSe-p3 are significantly higher (60% for e_{111} and 433% for e_{122}). To explain this effect and the modifications of ΔP_1 in the presence of Sn–Se vacancies, see Fig. 3(b) and (d), particularly the almost identical curves of SnSe-p4 and SnSe-p5 in contrast to that of SnSe-p3, we show in Fig. 3(f) histograms of the intralayer bond lengths (l_s and l_w) in the supercells. As expected, pristine SnSe shows two peaks of equal weight at 2.9 Å and 3.2 Å, while Sn–Se vacancies smear out the distribution. The two original peaks can still be recognised in the cases of SnSe-p4 and SnSe-p5 in contrast to the case of SnSe-p3, demonstrating that l_s and l_w, on average, are less similar for SnSe-p4 and SnSe-p5 than for SnSe-p3. Therefore, there is a strong correlation between the bond length disparity and the piezoelectric coefficients. Substantial structural relaxation in the cases of SnSe-s3 and SnSe-s4 results in negative e_{111} and e_{122}. SnSe-s4 shows the highest $|e_{111}|$ and $|e_{122}|$ among the Se vacancies, see Fig. 3(c) and (e), because the distribution of the intralayer bond lengths is smeared out most, see Fig. 3(g). Thus, the bond length disparity and piezoelectric coefficients are strongly correlated also in the case of Se vacancies. Reducing the bond length disparity, consequently, is an effective route to enhance the piezoelectric response in monolayer group IV monochalcogenides.

4. Conclusion

Our comprehensive investigation of the charge redistribution in monolayer group IV monochalcogenides under strain fully explains the trends of the piezoelectricity obtained in this family of materials. Charge transfer between the strong and weak intralayer bonds turns out to be the root cause of the piezoelectricity. Our results also suggest that the piezoelectric response is enhanced both by compressive strain and the presence of Sn–Se and Se vacancies, providing strategies to improve electro-mechanical devices.

Data availability

The data supporting this study are included in the article.

Conflicts of interest

There are no conflicts to declare.

Acknowledgements

We are grateful to Mohammed Ghadiyali and Shubham Tyagi for engaging discussions. The research reported in this publication was supported by funding from King Abdullah University of Science and Technology (KAUST). For computer time, this research used the resources of the Supercomputing Laboratory at KAUST.

References

1 Y. Nemirovsky, A. Nemirovsky, P. Muralt and N. Setter, Design of novel thin-film piezoelectric accelerometer, *Sens. Actuators, A*, 1996, **56**, 239.
2 S. Tadigadapa and K. Mateti, Piezoelectric MEMS sensors: State-of-the-art and perspectives, *Meas. Sci. Technol.*, 2009, **20**, 092001.
3 H. Bhugra and G. Piazza, *Piezoelectric MEMS resonators*, Springer, Berlin, 2017.
4 M. Pohanka, Overview of piezoelectric biosensors, immunosensors and DNA sensors and their applications, *Mater.*, 2018, **11**, 448.
5 D. Hu, M. Yao, Y. Fan, C. Ma, M. Fan and M. Liu, Strategies to achieve high performance piezoelectric nanogenerators, *Nano Energy*, 2019, **55**, 288.
6 N. Sezer and M. Koç, A comprehensive review on the state-of-the-art of piezoelectric energy harvesting, *Nano Energy*, 2021, **80**, 105567.
7 X. Gao, J. Yang, J. Wu, X. Xin, Z. Li, X. Yuan, X. Shen and S. Dong, Piezoelectric actuators and motors: Materials, designs, and applications, *Adv. Mater. Technol.*, 2019, **5**, 1900716.
8 A. Zaszczynska, P. Sajkiewicz and A. Gradys, Piezoelectric scaffolds as smart materials for neural tissue engineering, *Polymers*, 2020, **12**, 161.
9 C. Yang, J. Ji, Y. Lv, Z. Li and D. Luo, Application of piezoelectric material and devices in bone regeneration, *Nanomater*, 2022, **12**, 4386.
10 W. Wu, L. Wang, Y. Li, F. Zhang, L. Lin, S. Niu, D. Chenet, X. Zhang, Y. Hao, T. F. Heinz, J. Hone and Z. L. Wang, Piezoelectricity of single-atomic-layer MoS2 for energy conversion and piezotronics, *Nature*, 2014, **514**, 470.
11 H. Zhu, Y. Wang, J. Xiao, M. Liu, S. Xiong, Z. J. Wong, Z. Ye, Y. Ye, X. Yin and X. Zhang, Observation of piezoelectricity in free-standing monolayer MoS_2, *Nat. Nanotechnol.*, 2014, **10**, 151.
12 J. Zhang and S. Meguid, Piezoelectricity of 2D nanomaterials: Characterization, properties, and applications, *Semicond. Sci. Technol.*, 2017, **32**, 043006.
13 M. N. Blonsky, H. L. Zhuang, A. K. Singh and R. G. Hennig, Ab Initio prediction of piezoelectricity in two-dimensional materials, *ACS Nano*, 2015, **9**, 9885.
14 W. Li and J. Li, Piezoelectricity in two-dimensional group III monochalcogenides, *Nano Res.*, 2015, **8**, 3796.
15 R. Fei, W. Li, J. Li and L. Yang, Giant piezoelectricity of monolayer group IV monochalcogenides: SnSe, SnS, GeSe, and GeS, *Appl. Phys. Lett.*, 2015, **107**, 173104.
16 L. C. Gomes, A. Carvalho and A. H. Castro Neto, Enhanced piezoelectricity and modified dielectric screening of two-

dimensional group IV monochalcogenides, *Phys. Rev. B: Condens. Matter Mater. Phys.*, 2015, **92**, 214103.
17 Y. Dai, X. Zhang, Y. Cui, M. Li, Y. Luo, F. Jiang, R. Zhao and Y. Huang, Theoretical insights into strong intrinsic piezoelectricity of blue-phosphorus-like group IV monochalcogenides, *Nano Res.*, 2021, **15**, 209.
18 Y. Zhou, D. Wu, Y. Zhu, Y. Cho, Q. He, X. Yang, K. Herrera, Z. Chu, Y. Han, M. C. Downer, H. Peng and K. Lai, Out-of-plane piezoelectricity and ferroelectricity in layered α-In_2Se_3 nanoflakes, *Nano Lett.*, 2017, **17**, 5508.
19 M. T. Ong and E. J. Reed, Engineered piezoelectricity in graphene, *ACS Nano*, 2012, **6**, 1387.
20 S. Chandratre and P. Sharma, Coaxing graphene to be piezoelectric, *Appl. Phys. Lett.*, 2012, **100**, 023114.
21 F. Ahmadpoor and P. Sharma, Flexoelectricity in two-dimensional crystalline and biological membranes, *Nanoscale*, 2015, **7**, 16555.
22 Y. Gao, L. Zhang, G. Yao and H. Wang, Unique mechanical responses of layered phosphoruslike group-IV monochalcogenides, *J. Appl. Phys*, 2018, **125**, 082519.
23 F. Li, H. Chen, L. Xu, F. Zhang, P. Yin, T. Yang, T. Shen, J. Qi, Y. Zhang, D. Li and Y. Ge, Defect engineering in ultrathin SnSe nanosheets for high-performance optoelectronic applications, *ACS Appl. Mater. Interfaces*, 2021, **13**, 33226.
24 G. Kresse and D. Joubert, From ultrasoft pseudopotentials to the projector augmented-wave method, *Phys. Rev. B: Condens. Matter Mater. Phys.*, 1999, **59**, 1758.
25 R. D. King-Smith and D. Vanderbilt, Theory of polarization of crystalline solids, *Phys. Rev. B: Condens. Matter Mater. Phys.*, 1993, **47**, 1651.
26 N. A. Spaldin, A beginner's guide to the modern theory of polarization, *J. Solid State Chem.*, 2012, **195**, 2.
27 D. Vanderbilt, Berry-phase theory of proper piezoelectric response, *J. Phys. Chem. Solids*, 2000, **61**, 147.
28 S. Nag, A. Saini, R. Singh and R. Kumar, Influence of vacancy defects on the thermoelectric performance of SnSe sheet, *Phys. E*, 2021, **134**, 114814.
29 Y. Guo, H. Zhu and Q. Wang, Piezoelectric effects in surface-engineered two-dimensional group III nitrides, *ACS Appl. Mater. Interfaces*, 2018, **11**, 1033.
30 N. I. Atallah, M. E. Kemary, F. Pascale and K. E. E. Kelany, Extraordinary piezoelectric effect induced in two-dimensional rare earth monochalcogenides via reducing system dimensionality, *J. Materiomics*, 2023, **9**, 72.
31 Y. Chen, J. Liu, J. Yu, Y. Guo and Q. Sun, Symmetry-breaking induced large piezoelectricity in Janus tellurene materials, *Phys. Chem. Chem. Phys.*, 2019, **21**, 1207.
32 X. Wang, W. Shi and J. Wan, Enhanced piezoelectric effect in MoS_2 and surface-engineered GaN bilayer, *J. Appl. Phys.*, 2021, **130**, 015113.
33 N. Ghobadi, S. G. Rudi and S. S. Amiri, Electronic, spintronic, and piezoelectric properties of new Janus ZnAXY (A = Si, Ge, Sn, and X, Y = S, Se, Te) monolayers, *Phys. Rev. B*, 2023, **107**, 075443.
34 Y. Guo, J. Zhou, H. Xie, Y. Chen and Q. Wang, Screening transition metal-based polar pentagonal monolayers with large piezoelectricity and shift current, *npj Comput. Mater.*, 2022, **8**, 40.
35 J. George, G. Petretto, A. Naik, M. Esters, A. J. Jackson, R. Nelson, R. Dronskowski, G. M. Rignanese and G. Hautier, Automated bonding analysis with crystal orbital Hamilton populations, *ChemPlusChem*, 2022, **87**, e202200123.